The influence of historical sea-surface temperature patterns on regional precipitation trends

Jaydeep R. Pillai[1] , Kyle C. Armour[1,2], and David S. Battisti[1]

[1]*Department of Atmospheric and Climate Science, University of Washington, Seattle, Washington*

[2]*School of Oceanography, University of Washington, Seattle, Washington*

Corresponding author: Jaydeep R. Pillai, jpillai@uw.edu

ABSTRACT: State-of-the-art coupled global climate models (GCMs) fail to simulate key features of observed seasonal precipitation trends since 1980, including drying of the southwestern US, the southeastern US, East Africa, and subtropical South America, as well as wetting of the Maritime Continent and the Amazon. They also fail to simulate the sea-level pressure (SLP) trends since 1980 associated with a poleward shift of the North Pacific storm track in the mid-latitudes and a strengthened Pacific Walker Circulation. We show that state-of-the-art atmosphere-only climate model ensembles driven by observed sea-surface temperatures (SSTs) simulate historical precipitation and SLP trends that are more similar to those observed in the regions noted above, suggesting that the observed pattern of SST changes has shaped regional precipitation and SLP trends. Analysis of the coupled and atmosphere-only model ensembles reveals that multidecadal SST patterns similar to those of the interannual El-Niño Southern Oscillation are responsible for some of the regional trends simulated. A strengthening tropical Pacific zonal SST gradient is found to have contributed to observed drying over the southwestern US, subtropical South America, and the southeastern US, as well as observed wetting over the Maritime Continent, signifying a key role for tropical Pacific warming patterns in future precipitation trends in these regions.

1. Introduction

Global warming due to increasing concentrations of greenhouse gases is expected to produce substantial changes in the hydrological cycle around the world, affecting the regional distribution of precipitation (Douville et al. 2021) with major implications for snow cover (Adam et al. 2009), terrestrial and marine ecosystems (Weltzin et al. 2003; Doney et al. 2012), water availability (Konapala et al. 2020), and soil moisture (Seneviratne et al. 2010). Substantial seasonal precipitation trends have been observed and studied over recent decades including in the southwestern United States (US; e.g. Lehner et al. 2018; Seager and Hoerling 2014; Cayan et al. 2010; Williams et al. 2022), the southeastern US (Easterling et al. 2017; Qian et al. 2024), the Amazon Rainforest (Gloor et al. 2015; Almeida et al. 2016; Moreira et al. 2024), East Africa (Rowell et al. 2015; Gebrechorkos et al. 2019), and other regions.

Figure 1 (left column) illustrates the seasonal precipitation trends over the period 1979-2014 from the Global Precipitation Climatology Project (GPCP) dataset (see Section 2a for details). In the Northern Hemisphere, there have been drying trends over the southwestern and southeastern US in December-January-February (DJF) and March-April-May (MAM), a drying trend in East Africa in MAM, a wetting trend over the Maritime Continent during MAM, and wetting trends over the Sahel region in June-July-August (JJA) and September-October-November (SON). Over the Amazon, there has been a strong wetting trend in MAM and a drying trend in SON. There has also been a drying trend in subtropical South America during MAM.

Figure 1 (left column) also illustrates seasonal trends in sea-level pressure (SLP; black contours) calculated from a state-of-the-art atmospheric reanalysis (ECMWF ERA5; Hersbach et al. 2020) over the same period (see Section 2a). In the mid-latitudes, trends in SLP reveal changes in the average position of the storm tracks that bring precipitation to land regions (Trenberth et al. 1998). In the tropics, trends in SLP reveal changes in the areas of deep convection and weak subsidence, corresponding to regions of strong and weak precipitation, respectively. These figures illustrate a strong increase in SLP in the north Pacific during DJF and MAM, an increase in SLP in the south-central Pacific in MAM, JJA, and SON, and a decrease in SLP in the Pacific sector of the Southern Ocean in MAM, JJA, and SON. A zonally uniform decrease in SLP is also present in the Southern Ocean during DJF (Fan et al. 2014). There are strong SLP trends in the northern and southern Atlantic Ocean during DJF and SON. Finally, there has been a weak increase in SLP over the eastern equatorial Pacific in all seasons and a decrease in SLP over the Maritime Continent (a strengthening of the Pacific Walker Circulation), during MAM and SON. Altogether, the observed patterns of precipitation and SLP changes over recent decades show large regional trends with distinct seasonality.

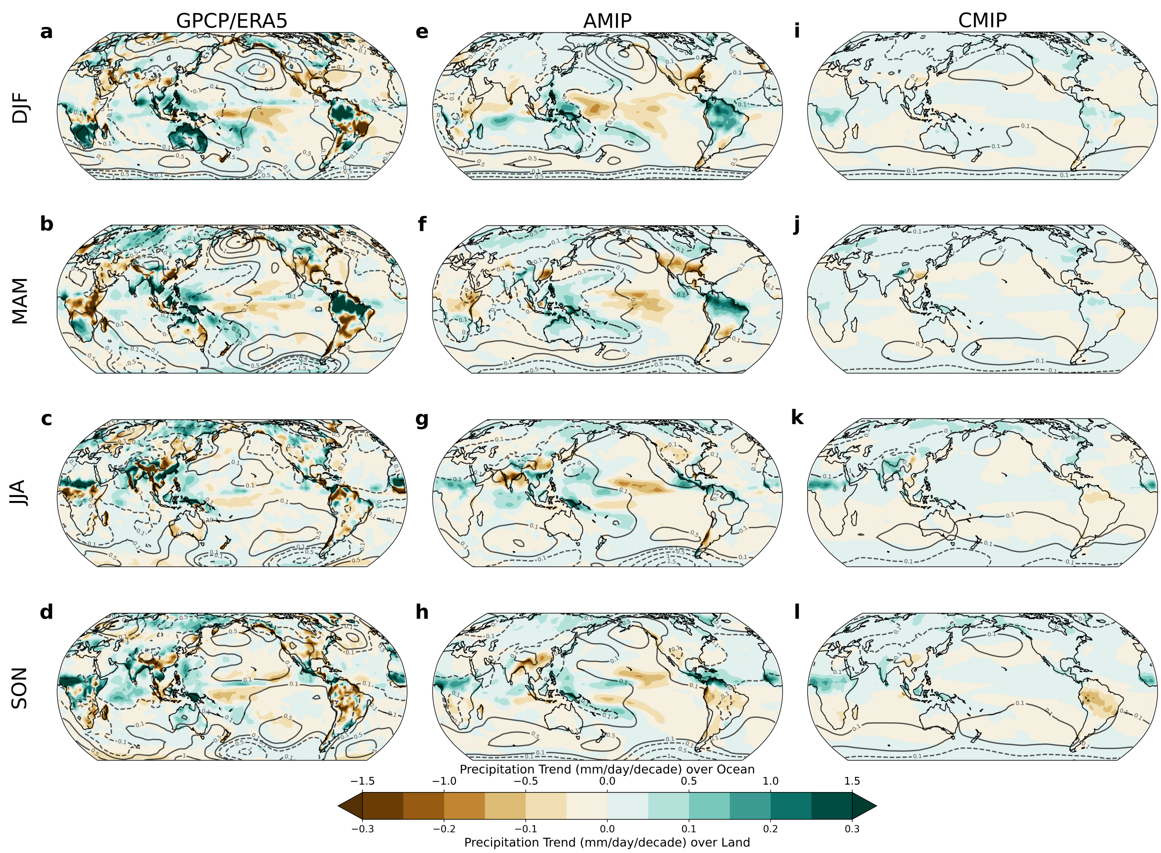

FIG. 1. Seasonal trends in precipitation and sea-level pressure (SLP) over 1979-2014 from (left, a-d) GPCPv2.3/ERA5 Reanalysis, (middle, e-h) multi-model mean AMIP simulations, and (right, i-l) multi-model mean CMIP simulations. Simulations from the same model are averaged before averaging over all model ensembles (see Eqs. 1a, 1b). Trends in precipitation over ocean and land use separate colorbar scalings. SLP contour lines are (0.1, 0.5, 1, 1.5, and 2) hPa / decade (dashed contours are negative, zero contour is omitted).

What has driven these observed precipitation and SLP trends? Climate models can serve as a guide. Figure 1 (right column) shows 1979-2014 precipitation trends averaged over selected global climate models (restricted to those providing many ensemble members; see Section 2b and Table 1) participating in phases 5 and 6 of the Coupled Model Intercomparison Project (CMIP5, Taylor et al. 2012; CMIP6, Eyring et al. 2016). These precipitation trends represent the forced response of the fully-coupled (CMIP) models to historical changes in greenhouse gases and other forcing agents over the same period as the observations. The CMIP model forced response largely fails to reproduce observed trends in precipitation in many regions and seasons, even simulating an incorrect sign of trends in some regions, such as in the southeastern US during DJF and MAM, East Africa during MAM, and subtropical South America during MAM.

That coupled models forced by historical forcing generally fail to reproduce observed precipitation trends (albeit over earlier time periods) has been noted by Hoerling et al. (2010), Seager and Vecchi (2010), and Shin and Sardeshmukh (2011), indicating that these differences have persisted for multiple climate model generations. Knutson and Zeng (2018) and Vicente-Serrano et al. (2022) also find that coupled models with historical forcing do not reproduce observed precipitation trends: the former suggested that CMIP5 models have a tendency to underestimate the observed precipitation trends, and the latter showed that CMIP6 models do not improve upon the deficiencies of CMIP5 models in simulating precipitation trends (see also Donat et al. 2023). The CMIP models also generally fail to reproduce the observed spatial pattern and magnitude of trends in SLP over many regions and seasons (Simpson et al. 2025). Notably they do not reproduce the observed strengthening of the Pacific Walker circulation (Chung et al. 2019; Wills et al. 2022; Kociuba et al. 2015), increasing wintertime Southern Hemisphere storminess (Chemke et al. 2022; Shaw et al. 2022; Kang et al. 2024), or strengthening of the wintertime North Atlantic jet (Blackport and Fyfe 2022; Bracegirdle et al. 2018).

The mismatch between the ensemble averaged forced CMIP precipitation and SLP trend patterns and those observed (see Fig. 1) does not necessarily indicate that the models' forced response is wrong, given that observations reflect only a single realization of internal climate variability. Observations of sea-surface temperature (SST) trend patterns have been shown to differ substantially from the forced SST trends simulated by CMIP models (Wills et al. 2022). In particular, observations have shown a large-scale cooling trend in the central-eastern Pacific Ocean and a warming trend in the western tropical Pacific Ocean in all seasons – a strengthening of the east-west (zonal) equatorial SST gradient that broadly resembles a trend toward La Niña-like conditions (Fig. 2). Studies show that atmospheric general circulation models forced by the observed tropical Pacific SST trends better reproduce the observed precipitation trends over North America (Seager and

Hoerling 2014; Delworth et al. 2015; Siler et al. 2019; Seager et al. 2023; Qiu et al. 2024; Kang et al. 2025), implying that the inability of the CMIP model forced response to capture observed SLP and precipitation trends in those regions may be traced to their inability to capture the observed tropical SST trend patterns (e.g., Wills et al. 2022). The question arises: can CMIP model biases in SLP and precipitation trends in other regions also be traced to their biases in tropical SST trend patterns?

Here, we study the global influence of historical SST trend patterns on regional precipitation trends since 1979. To do so, we compare precipitation and SLP trends simulated using fully-coupled CMIP models with both observations and trends simulated as part of the Atmospheric Model Intercomparison Project (AMIP; Taylor et al. 2012; Eyring et al. 2016), wherein atmospheric model simulations are performed using the same historical radiative forcing as in the fully-coupled CMIP models, but with observed SSTs and sea-ice concentrations prescribed.

Figure 2 shows the multimodel mean SST trends for AMIP (left column) and CMIP (middle column) for the same set of models over 1979-2014. The AMIP simulations (with SSTs prescribed from observations) prescribe a broad cooling trend in the central-eastern Pacific and warming in the western Pacific in all seasons. The AMIP simulations also prescribe a cooling trend in the Southern Ocean and warming throughout the rest of the oceans. In contrast, the CMIP models simulate more uniform warming across all ocean basins. The right column of Fig. 2 shows the difference between CMIP-simulated and AMIP (observed) SST trends, highlighting large discrepancies throughout the Pacific and Southern Oceans.

The middle column of Fig. 1 (e-h) shows the precipitation and SLP trends in the AMIP simulations. The AMIP simulations show a broad improvement in simulating observed regional precipitation and SLP trends compared to the coupled model (CMIP) forced response. In the Northern Hemisphere, the AMIP simulations capture the observed drying trends in the southwestern and southeastern US during DJF and MAM, the drying trend in East Africa during MAM, the wetting trend over the Maritime Continent during DJF, MAM, and SON, and the wetting trend over the Sahel during SON. In the Southern Hemisphere, the AMIP models capture the observed wetting trend over the Amazon in MAM and the drying trend over the Amazon during SON. The AMIP SLP trends also better resemble those from the ERA5 reanalysis, with large positive trends in the North Pacific during DJF and MAM, as well as negative trends in the Southern Ocean during

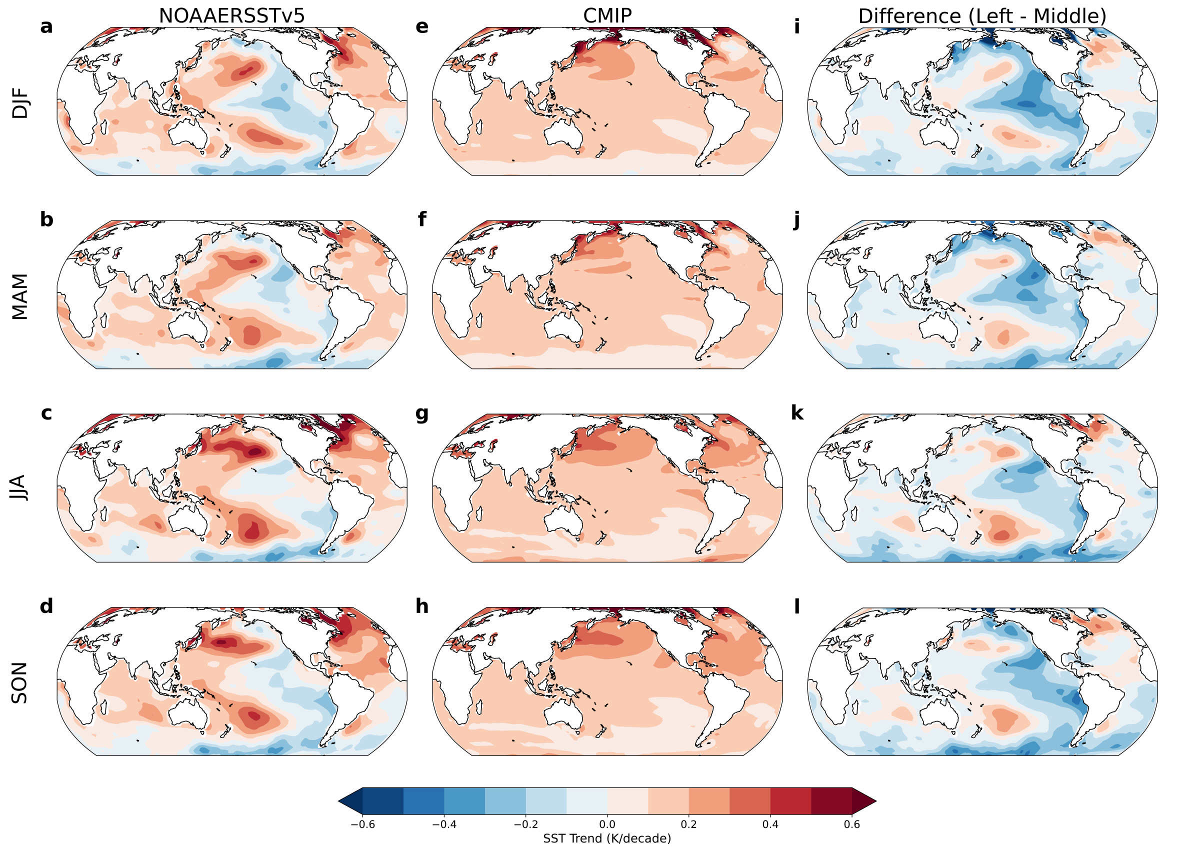

FIG. 2. Seasonal trends in sea-surface temperature (SST) over 1979-2014 from (left, a-d) observations used to force the AMIP simulations, (middle, e-h) multi-model mean CMIP simulations, and (right, i-l) the difference between AMIP and CMIP simulations. Simulations from the same CMIP model are averaged before averaging over all model ensembles (see Eqs. 1a, 1b).

DJF, JJA, and SON. Recent work has similarly demonstrated how prescribing SST trends in models substantially improves the simulation of these precipitation and large-scale circulation trends (Gu and Adler 2023; Kang et al. 2025; Yeager et al. 2023), with implications for future projections and higher-impact climate metrics such as storm-statistics (Zhao and Knutson 2024).

Given that the AMIP and CMIP models are driven by identical historical radiative forcing, and differ only in their SST patterns, these findings (Figs. 1 and 2) suggest that the unique pattern of observed SST trends has indeed contributed to the observed trends in regional precipitation and SLP in several regions and seasons around the world. However, key questions remain: 1) How well do AMIP simulations capture observed precipitation trends? 2) Are the mechanisms linking

SST trend patterns to precipitation and SLP trends over recent decades the same as those linking SST patterns to precipitation and SLP changes on interannual timescales (e.g., mediated by the well-understood atmospheric dynamics associated with the El Niño Southern Oscillation, ENSO)? 3) What role does the tropical Pacific zonal SST gradient play in shaping precipitation trends? Answering these questions is the aim of this study, with implications for understanding historical precipitation trends and predicting precipitation changes as the SST pattern evolves in the future.

The outline of this paper is as follows: Section 2 describes the datasets and methods used. Section 3 describes the analysis and results in five parts: the criteria for regional analysis (Section 3a); observed and modeled SST/sea-level-pressure/precipitation teleconnections on interannual timescales (Section 3b); an evaluation of whether teleconnections associated with interannual variability also mediate long-term precipitation and circulation trends (Section 3c); the role of differences between observed and simulated SST trends in influencing regional precipitation trends (Section 3d); and a discussion of why some regions' precipitation may not be influenced by the unique pattern of observed SST trends (Section 3e). Finally, we discuss implications for future precipitation trends, with a focus on regions where the tropical Pacific has had a dominant influence on precipitation trends in recent decades.

2. Data & Methods

a. Observations and reanalysis data

For observed precipitation, we use the Global Precipitation Climatology Project version 2.3 (GPCP, Adler et al. 2018). GPCP provides near-global coverage of precipitation by blending observations from rain gauges and satellites since 1979. These data are monthly means with a resolution of 2.5° latitude × 2.5° longitude, and are the main observed precipitation dataset used for Sections 3a-d. In Section 3d, we compare the results with two other precipitation products: the National Oceanic and Atmospheric Administration Climate Prediction Center Merged Analysis of Precipitation (NOAA CMAP, Xie and Arkin 1997) and the Global Precipitation Climatology Centre Full Data Reanalysis (GPCC, Schneider et al. 2022). The NOAA CMAP product, much like the GPCP product, combines near-global satellite coverage with rain gauge measurements of monthly mean precipitation, starting in 1979 and continuing to the present with a resolution of 2.5° latitude × 2.5° longitude. The GPCC product is composed of weather station measurements of monthly mean precipitation from 1891 through 2019 at a resolution of 2.5° latitude × 2.5° longitude.

For SLP, we use the ECMWF Reanalysis version 5 (ERA5; Hersbach et al. 2020). These data are also monthly means from January 1979 to the present, with a resolution of 0.25° latitude × 0.25° longitude. For observed SSTs, we use the National Oceanic and Atmospheric Administration Extended Reconstruction Sea-Surface Temperature version 5 (ERSSTv5, Huang and Coauthors 2017), a 2.0 ° latitude × 2.0° longitude monthly gridded dataset extending from January 1854 to the present. We conduct our analyses over the period 1979–2014 to coincide with the start of the satellite era (1979) and the end of the most recent publicly available AMIP simulations (2014).

b. Climate model data

Isolating the forced response of a climate model requires a large ensemble of simulations that can be averaged to reduce the influence of internal variability. Each ensemble member is initialized from a perturbed set of initial conditions and evolves under the same radiative forcing. For each CMIP model, we analyze the corresponding AMIP model, which is composed of the same atmosphere and land module as its CMIP counterpart. Each AMIP model ensemble is forced with the same radiative forcing as its CMIP counterpart, but has observed SSTs and sea-ice concentrations prescribed as surface boundary conditions. Individual AMIP ensemble members are also initialized from a perturbed set of initial conditions, producing an estimate of internal atmospheric variability that occurs given the same prescribed SSTs, sea-ice conditions, and radiative forcing. Averaging over the ensemble members of CMIP model large ensembles provides an estimate of the climate response to historical forcing. Meanwhile, averaging over the ensemble members of the AMIP model ensembles provides an estimate of the climate response to historical forcing subject to the observed timeseries of SSTs and sea-ice concentrations. Table 1 outlines the CMIP and AMIP models used (8 in total), as well as the number of members constituting each ensemble.

We analyze monthly mean precipitation, SLP, and SST fields from the CMIP and AMIP *historical* forcing simulations. For models where SST data could not be found, we analyze surface temperature (model variable *TS*) data masked by land and we omit high-latitude areas under sea-ice cover. All data were downloaded from the Earth System Grid Federation (Cinquini et al. 2014) and the

CMIP Model (members)	AMIP Model (members, End Date)	References
CESM1.1 (40)	CAM5-GOGA (10, 2015)	Kay et al. (2015)
CanESM2 (50)	CanAM4 (5, 2009)	Kirchmeier-Young et al. (2017), von Salzen et al. (2013)
GFDL-CM3 (20)	GFDL-CM3 AMIP (5, 2008)	Sun et al. (2018)
MPI-ESM-LR (100)	ECHAM6 (3, 2008)	Maher et al. (2019)
EC-Earth (16)	EC-Earth AMIP (1, 2008)	Hazeleger et al. (2010)
CESM2(CMIP6 Forcing) (50)	CAM6-GOGA (10, 2021)	Rodgers et al. (2021)
MIROC6 (50)	MIROC6 AMIP (10, 2014)	Tatebe et al. (2019)
MPI-ESM1.2-LR (50)	MPI-ESM1.2-LR AMIP (3, 2014)	Olonscheck et al. (2023)

Table 1. CMIP large ensembles (and corresponding AMIP ensembles) used for analysis as well as the number of members (N) used within each ensemble.

National Center for Atmospheric Research Climate Data Gateway (NCAR CDG). The precipitation data include both liquid and solid phase and both convective and large-scale precipitation.

Some AMIP simulations from the CMIP5 generation of models end before December 2014. Linear trends calculated are still scaled by 10 years, and regional analysis is performed in areas where our results do not change with respect to varying start and end dates. For the CMIP5 (coupled) simulations of historical forcing and the CAM5-GOGA simulations (both ending in 2006), we append model output from the Representative Concentration Pathways (RCP) 8.5 scenario to 2014, justified by Schwalm et al. (2020) who demonstrate that RCP8.5 scenario CO_2 emission forcing estimates match that of observed cumulative carbon dioxide emissions until the year 2020.

c. Methods

1) Model ensemble averaging

To motivate regions for the analysis of precipitation, we calculate the linear trends in 3-month-average precipitation, SLP, and SST for observations/reanalysis, AMIP ensembles, and CMIP ensembles, sliding the 3-month average every month. For each of the CMIP and AMIP models, we calculate the ensemble average trends as:

$$\overline{S}_j = \frac{1}{N_j} \sum_{k=1}^{N_j} S_{jk}, \tag{1a}$$

where N_j is the number of ensemble members for model j, and S_{jk} is the trend in precipitation/SLP for ensemble member k. Averaging over all models:

$$\langle S \rangle = \frac{1}{M}\sum_{j=1}^{M}\overline{S}_j, \tag{1b}$$

where $M = 8$ is the total number of models, and $\overline{S}_j$ is the average trend over model j. We calculate all subsequent ensemble and model averages using Eqs. (1a, 1b). Figure 1 shows the precipitation and SLP results for meteorological seasons DJF, MAM, JJA, and SON. In this approach, each model ensemble is weighted equally to avoid favoring models with many ensemble members. Weighting each ensemble member equally across all models produces similar results. All data are regridded to a common $2.5° \times 2.5°$ rectilinear grid before analysis.

2) Measuring atmospheric variability

In Section 3a, we compute the difference in the modeled 3-month average trends in precipitation from the GPCP trends, and also compute the difference between the AMIP and CMIP ensembles. We normalize these differences by a measure of the spread in precipitation trends associated with intrinsic atmospheric variability, σ_{AMIP}, estimated as follows. First, we calculate the standard deviation of precipitation trend across the ensemble members of each AMIP model:

$$\sigma_j = \sqrt{\frac{1}{N_j}\sum_{k=1}^{N_j}(S_{jk} - \overline{S}_j)^2}, \tag{2}$$

where N_j is the number of ensemble members in a given model, j is the model, $\overline{S_j}$ is the mean precipitation trend for model j, and S_{jk} is the trend of an individual ensemble member in precipitation. We then average the σ_j^2 over all the models to obtain σ_{AMIP}:

$$\sigma_{AMIP} = \sqrt{\frac{1}{M}\sum_{j=1}^{M}\sigma_j^2}. \tag{3}$$

σ_{AMIP} represents the the standard deviation in precipitation trends due to internal atmospheric variability when SSTs and sea ice are prescribed (i.e., that arising from chaotic atmospheric motions). σ_{AMIP} provides a measure of how closely we could ever expect climate model simulations to capture observed precipitation trends, given that those trends reflect a single realization of intrinsic atmospheric variability. When differences between modeled and observed trends are much larger than σ_{AMIP}, those differences cannot be attributed to internal atmospheric variability and thus reflect a robust difference. However, when differences between modeled and observed trends are smaller than σ_{AMIP}, then those differences might have arisen from intrinsic atmospheric variability in the observations, and we thus regard them as in agreement.

3) Regressing across Ensemble Member Trends

In Section 3c, we estimate how variations in SST and SLP trends across ensemble members relate to variations in regional precipitation trends using ordinary least-squares regression. In this approach, each ensemble member from a CMIP model ensemble provides an area-averaged precipitation trend from the regions listed in Table 2, an SST trend field, and an SLP trend field; we regress the SST and SLP trend fields against the precipitation trend across ensemble members to isolate the linear component of their co-variability. Let P be a trend in area-averaged precipitation, and T_i be a trend in SST or SLP at gridpoint i. For a given model with N ensemble members, there are N trends in both P and T_i. Then, we can write the regression coefficient at each gridpoint as:

$$\beta_i = \frac{\sum_{k=1}^{N} P'_k T'_{k,i}}{\sum_{k=1}^{N} (P'_k)^2}, \tag{1}$$

where prime denotes deviation from the mean and k is an index over the N ensemble members of a model. This coefficient describes how strongly the SST or SLP trend at grid point i varies linearly with the precipitation trend across a CMIP model ensemble.

4) Equatorial Pacific SST Gradient Calculation

In Section 3d, we quantify the role of the evolving equatorial Pacific SST gradient on regional precipitation. We calculate the SST gradient as

$$SST_{W-E} = SST_W - SST_E, \tag{4}$$

where SST_W is SST averaged over ($5°S$ - $5°N$, $110°E - 180°$) and SST_E is SST averaged over ($5°S$ - $5°N$, $180°$ - $80°W$). We calculate the trend in SST_{W-E} for each member of each CMIP model ensemble over all of the seasons in Table 2. For each model, we regress the precipitation trend at each gridpoint against the SST_{W-E} trend from each ensemble member, obtaining a regression coefficient map for that model. We multiply the regression coefficient map by the observed SST_{W-E} trend (obtained from ERSSTv5) to obtain the portion of precipitation trend over the period 1979-2014 attributable to multi-decadal changes in the equatorial SST gradient for each model.

3. Analysis

a. Identifying regions and seasons of interest based on observed and simulated precipitation trends

Figure 1 showed precipitation trends from observations (GPCP), AMIP models, and CMIP models. Figure 3 shows the difference between GPCP, AMIP, and CMIP trends, normalized by σ_{AMIP} for each season to illustrate where the differences are large compared to trends that can occur due to intrinsic atmospheric variability alone, which we use as a measure of significance. The right column of Fig. 3 shows differences in precipitation trends between AMIP and CMIP models. Because AMIP and CMIP models are driven by identical historical radiative forcing, any large differences in their precipitation trends can be attributed to differences between the observed and CMIP-simulated patterns of SST trends.

1) Identifying regions of interest

We highlight eight land regions of interest with either red or dashed magenta boxes (Fig. 3). Red boxes indicate regions where 1) CMIP models show geographically coherent differences from the observed precipitation trends, 2) AMIP models show a substantially smaller bias than the CMIP models compared to the observed trends, and 3) AMIP models correctly simulate the sign of the observed trend. The red boxes thus illustrate regions where the observed precipitation trend is in large part explained by the unique pattern of SST trends observed over recent decades, rather than by the forced response to historical forcing.

For example, in the southwestern US the CMIP model mean shows large and widespread precipitation trend biases during MAM, with the CMIP models simulating a weak drying trend that is over $2.0\sigma_{AMIP}$ from the observed strong drying trend (Figs. 3b and 1b). However, AMIP models simulate a strong drying trend that is in good agreement with the observed trend in this region (Fig. 3f). The difference between AMIP and CMIP responses (Fig. 3j) provides a measure of how the

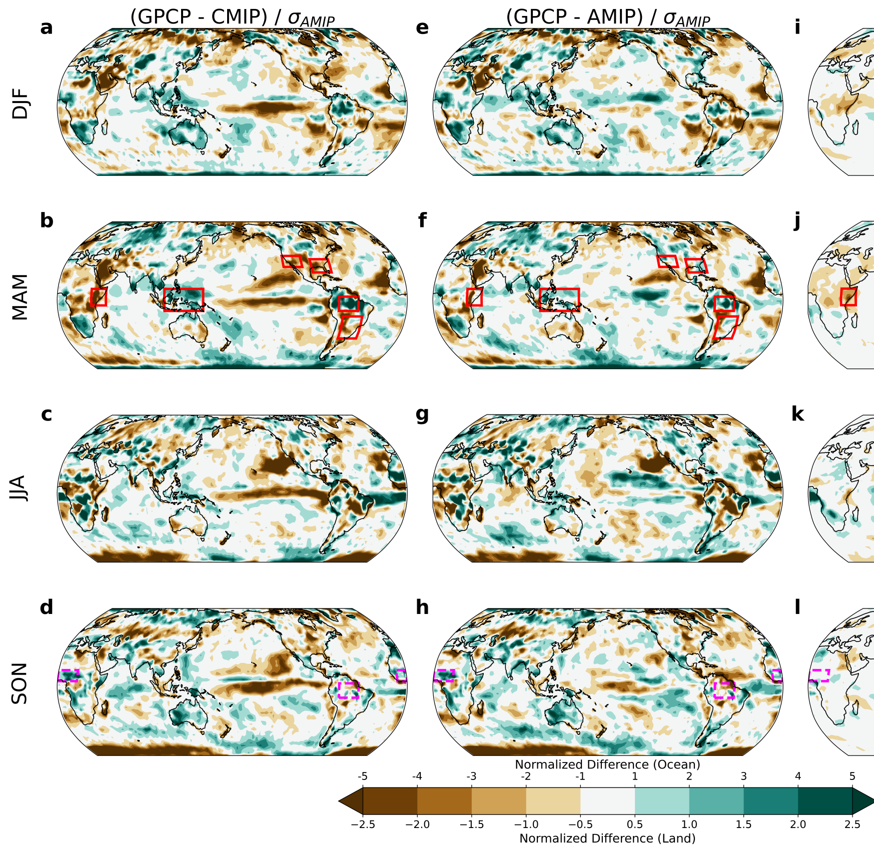

FIG. 3. Seasonal differences in precipitation trends over 1979-2014 normalized by the average standard deviation of precipitation trends in the AMIP ensembles (σ_{AMIP}). Comparing (left) GPCP to CMIP model forced response, (middle) GPCP to AMIP model forced response, and (right) the difference between AMIP and CMIP model forced responses. Darker colors illustrate where differences are large compared to internal atmospheric variability, while white illustrates where differences are small compared to internal atmospheric variability. Red boxes highlight regions where AMIP models show substantially smaller biases in the simulated trend and simulate the correct sign of the observed change, indicating that the observed precipitation trend is in part due to observed SST trends that differ from the forced CMIP SST trend. Magenta dashed boxes indicate regions in seasons where the CMIP and AMIP models both capture the sign and relative magnitude of the observed precipitation trend, indicating that the difference between observed and CMIP-simulated SST trends does not significantly influence precipitation trends there.

unique observed SST pattern has influenced precipitation trends: it has contributed substantially to the strong drying trend over the southwest US in MAM.

A similar story can be seen in other regions as well. In the southeastern US in MAM, the CMIP models simulate a wetting trend that is over $2.5\sigma_{AMIP}$ from the observed strong drying trend (Figs. 3b and 1b), while AMIP models simulate a drying that is in much better agreement with observations (Figs. 3b, f). In East Africa during MAM, the CMIP models simulate a weak wetting trend that is over $2.5\sigma_{AMIP}$ from the observed strong drying trend (Figs. 3b and 1b), and AMIP models simulate a drying trend that is in better agreement with observations, except over high-elevation regions (Fig. 3f). Over the Maritime Continent, the CMIP models simulate a weak precipitation trend that is $2.0\sigma_{AMIP}$ from the observed wetting trend in MAM, while AMIP models simulate a wetting trend that is in good agreement with observations (Fig. 3f). In South America over the Amazon Rainforest during MAM, the CMIP models simulate a weak drying trend that is over $2.5\sigma_{AMIP}$ from the observed wetting trend (Figs. 3b and 1b,j), while AMIP models simulate a wetting trend that is in better agreement with observations (Fig. 3f). In subtropical South America during MAM the CMIP models simulate a weak wetting trend that is around $2.0\sigma_{AMIP}$ from the observed drying trend (Figs. 3b and 1b), while AMIP models simulate a drying trend that is improved compared to observations, but still biased by $1.5\sigma_{AMIP}$ (Fig. 1f). While the difference between the AMIP and CMIP simulated trend in subtropical South America is small, adjusting the seasons (see Section 3a.2) magnifies the difference and justifies our analysis of this region. In each of these regions, the difference between AMIP and CMIP responses suggests that the unique observed SST trend pattern has played a key role in the observed MAM precipitation trends (Fig. 3j).

In contrast, dashed magenta boxes on Fig. 3 highlight regions where both the CMIP and AMIP models simulate precipitation trends that are similar in magnitude and sign to the observed trend. In these regions, processes other than the difference between the observed and CMIP-simulated SST patterns dominate the precipitation trend, such as the response to the common radiative forcing prescribed in both CMIP and AMIP models. We analyze two equatorial regions within the same season (SON) where this occurs: the Sahel and the Amazon. In the Sahel, both AMIP and CMIP models simulate wetting trends similar to those observed. Normalized differences (Fig. 3l) indicate that the AMIP and CMIP models agree on the magnitude of simulated wetting. In the Amazon, AMIP and CMIP models simulate the observed drying trend, with the CMIP models simulating a stronger trend than the AMIP models. In these two regions, the similarity between AMIP and

CMIP responses suggests that the unique observed SST trend pattern has not played a role in the observed SON precipitation trends (Fig. 3l).

Additional regions also show large normalized differences between the CMIP and AMIP simulations (right column of Fig. 3). However, we choose not to analyze these regions because (i) the magnitude of the trend differences between observations, CMIP models, and AMIP models are small, such is the case for the southern portion of Africa during JJA, or (ii) the observed trends are not robust with respect to varying start and end dates, such is the case with the Maritime Continent during SON and DJF. In the analysis that follows, we focus on the eight (red and magenta boxed) regions in Fig. 3.

2) Identifying seasons of interest

Location	Months	Trend (mm/day/decade)	SSTs Matter? (Fig. 3)	tropical Pacific SST_{W-E} Matters? (Fig. 7)
Southwestern United States	JFMA	-0.14	✓	✓
Southeastern United States	JFMA	-0.22	✓	✓
East Africa	MAM	-0.25	✓	×
Maritime Continent	MAM	0.39	✓	✓
Subtropical South America	AMJ	-0.09	✓	✓
Amazon	FMAM	0.35	✓	×
Amazon	ASON	-0.11	See Section 3e	×
Sahel	ASON	0.25	See Section 3e	×

Table 2. Locations and seasons analyzed for this study, along with the observed area-averaged trend in precipitation for 1979-2014 (from GPCPv2.3). Check marks indicate the global pattern of SST trends and the tropical Pacific zonal SST gradient trend influence the precipitation trend in that region.

For each of the regions highlighted in Section 3a(1), we adjust the seasons of interest by calculating sliding 3-month average (DJF, JFM, FMA, ... etc.) normalized differences in precipitation trends. Starting from the meteorological seasons highlighted above in Section 3a, we include neighboring months that strengthen the observed precipitation trends while excluding months that weaken trends. For example, in the southwestern US during MAM, we remove May since it diminishes the drying signal, while adding January and February since they contribute to a stronger drying over the 36-year period. Table 2 lists the adjusted seasonal average analyzed for each region in the rest of the analysis and also summarizes whether the global trend pattern in SST and the trend in the tropical Pacific zonal SST gradient contributed to the long-term trends in precipitation (Section 3d).

b. The SST-precipitation relationship on interannual timescales

Figure 1 and the red boxes in 3 show where AMIP models, given the observed SST trend pattern, simulate improved precipitation trends in key regions and seasons compared to CMIP models. Previous literature (Seager and Hoerling 2014, Lehner et al. 2018, Siler et al. 2019, Qiu et al. 2024) suggests that tropical SSTs are important in driving some of the regional trends. Here we explore which SST patterns are connected to precipitation and SLP changes for each of our regions and seasons of interest on the interannual timescale in both observations and models. This analysis will allow us to evaluate how well models simulate observed atmospheric teleconnections, and provide context for why model simulations may or may not capture observed trends in precipitation and atmospheric circulation in Section 3c.

To study the links between SSTs, SLP, and regional precipitation on interannual timescales, linearly detrended ensemble members from each model are concatenated for both AMIP and CMIP models (the observed records of SST, SLP, and precipitation are also linearly detrended). Seasonal anomalies are calculated as departures from climatology, and precipitation anomalies are normalized by their standard deviation before spatially averaging over each region of interest (see again Table 2). SST and SLP anomaly fields are then regressed upon the regionally-averaged normalized precipitation, producing regression maps of SST and SLP patterns associated with the precipitation anomalies. We control for the false discovery rate using the method of Wilks (2016) at level $\alpha = 0.1$ (see Benjamini and Hochberg 1995 for a more in-depth explanation) and stipple SST at each gridpoint (and blacken SLP contours) if five or more models agree on significance. For observations we stipple if Wilks 2016's method deems the gridpoint significant. Figure 4 shows the regression maps, where regression values are scaled by -1 to reflect drying in the boxed region.

For observations (left column of Fig. 4), the importance of the tropical Pacific for many regions' precipitation reflects well understood ENSO teleconnections (Ropelewski and Halpert 1987; Trenberth et al. 1998; Davey et al. 2014): seasonal precipitation in the southwestern US (A1), the Maritime Continent (D1), subtropical South America (E1), and the Amazon (FMAM, F1) is

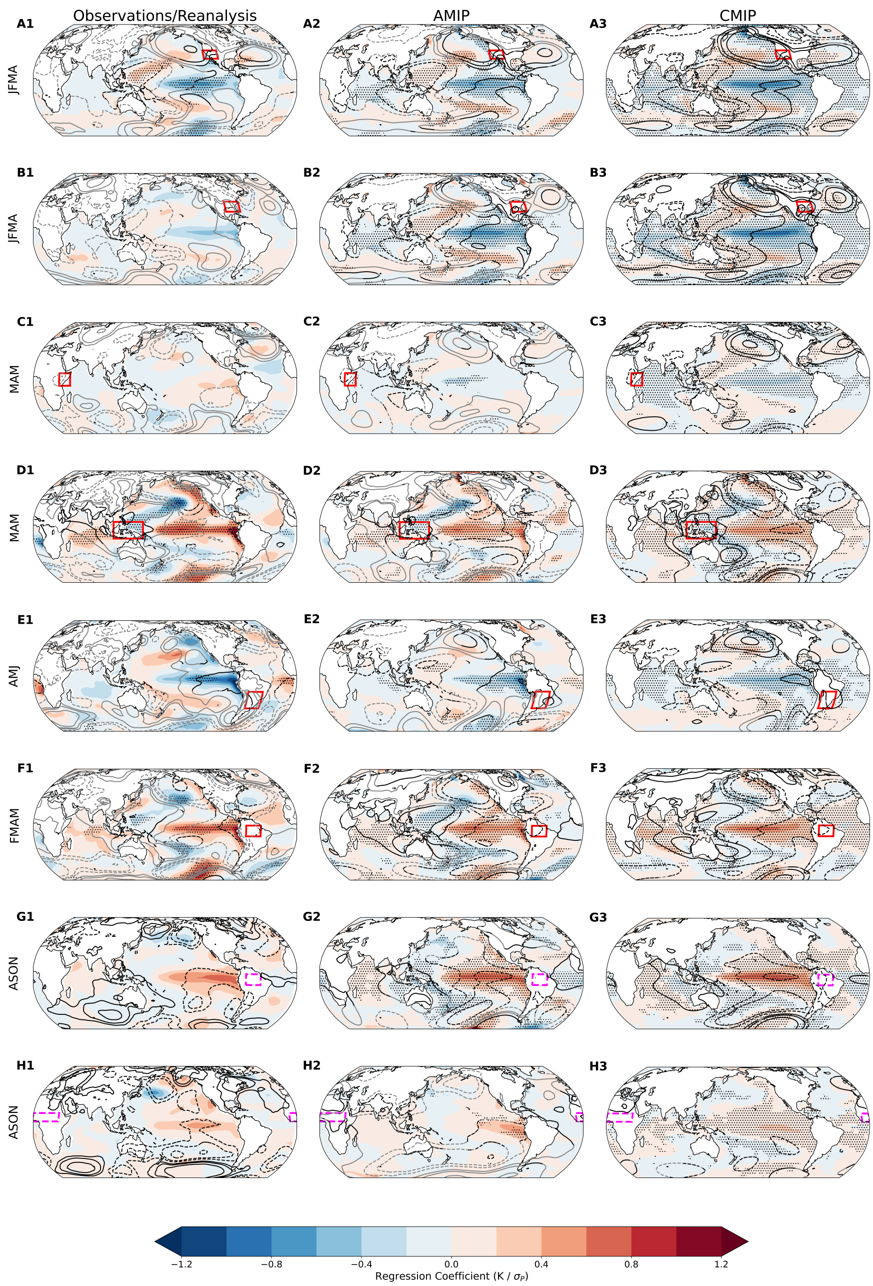

FIG. 4. Interannual anomalies in SST and SLP regressed on normalized precipitation anomalies (averaged over the red box in each figure) for observations/reanalysis (left column), AMIP models (center column) and CMIP models (right column). Significant relationships between SST anomalies and normalized precipitation are stippled, while significant relationships between SLP anomalies and normalized precipitation are shown in black contours (otherwise grey). Regression values are scaled by -1 to facilitate comparison with the La-Niña-like SST pattern from Figure 2. SLP contours are (0.25, 0.5, 1, 2, 3, and 5) hPa / σ_P (dashed contours are negative, zero contour is omitted).

modulated by interannual variability in tropical Pacific SST associated with ENSO. In the tropics, El-Niño conditions cause rainfall deficits in MAM in the Maritime Continent (D1) and in FMAM in the Amazon (F1). In the midlatitudes, poleward propagating Rossby waves generated by anomalous tropospheric latent heating from deep convection in the tropics affect the extratropical large-scale atmospheric flow. For the southwestern US, La Niña causes a poleward shift in the storm tracks, indicated by the strengthening SLP over the north Pacific, reflecting fewer storms reaching these regions (Fig. 4A1). Over subtropical South America, La Niña SST anomalies cause a wave train that shifts the Southern Hemisphere storm tracks poleward, reflecting reduced precipitation reaching this region as well (Fig. 4E1; Garreaud and Battisti 1999); previous literature has also commented on the large role of interannual tropical Pacific variability on precipitation in this region (Seager et al. 2010a).

Comparing the observed teleconnections to those in the AMIP and CMIP models, we find that the models simulate the observed relationship between precipitation and the patterns of SLP and SST in the southwestern US (Fig. 4 row A), the Maritime Continent (row D), subtropical South America (row E), and the Amazon in FMAM (row F). Most notably, statistically significant SST anomalies are located in the tropical Pacific for both observations and models and statistically significant SLP contours are consistent with tropical and midlatitude circulation shifts associated with ENSO. The observed relationships between SST, SLP and precipitation anomalies over the Amazon in ASON (row G) and the Sahel (row H) are also reproduced by the models. That models simulate strong SST anomaly patterns that are similar to those observed supports the conclusion that the observed relationships are meaningful teleconnections. Previous literature (Davey et al. 2014) indicates that La-Niña-like conditions can cause negative precipitation anomalies in the southeastern US, positive precipitation anomalies in the Amazon in ASON, and weak positive anomalies in the Sahel in ASON (Folland et al. 1991). However, the SLP anomalies associated with drying in each region only agree across models and observations for the Amazon in ASON. Previous literature also indicates that ENSO has no effect on East African precipitation in MAM (e.g., Davey et al. 2014). AMIP and CMIP ensembles suggest, unlike in observations (Fig. 4C1), that La Niña conditions contribute to weak precipitation deficits (Fig. 4C2,3) in this region, possibly owing to the much longer time series analyzed in each model (N ensemble members $\times$ 36 years) compared to observations (36 years).

In summary, we have shown which SSTs matter for precipitation anomalies in the boxed regions of Fig. 3 on interannual timescales. Consistent with previous studies, observations show that SST variability in the tropical Pacific affects precipitation in 6 of 8 regions considered here, indicating the importance of ENSO variability for precipitation in these regions. Our analysis also shows that AMIP and CMIP models reproduce the strong relationships observed between tropical Pacific SST, global SLP, and precipitation anomalies in each of these regions (although the relationship between SST, SLP, and regional precipitation in observations is not statistically significant in some regions, possibly owing to the short record length).

c. The SST-precipitation relationship on multidecadal timescales

The previous section established the ability of models to simulate well-understood, observed SST-precipitation teleconnections modulated by changes in atmospheric circulation on interannual timescales. In this section, we examine the multidecadal trends (1979-2014) in the CMIP models to assess whether the observed trends could arise due to internal (unforced) SST variability, and if so, whether the processes responsible are related to trends in tropical Pacific SSTs. Previous literature has shown that SST trends can affect long-term precipitation trends, particularly in the southwestern US. For example, Lehner et al. (2018) and Siler et al. (2019) used dynamical adjustment to understand how tropical Pacific SSTs have influenced recent trends in western US precipitation and SLP, while Qiu et al. (2024) found that tropical SST trends contribute to precipitation trends over the southwestern US and Amazon regions (see also Seager et al. 2023; Delworth et al. 2015). Kuo et al. (2023, 2025) point to the role of anthropogenic aerosols driving SST and circulation trends that influence southwestern US precipitation. Elsewhere, Rowell et al. (2015) and Schwarzwald and Seager (2024) compared CMIP and AMIP model precipitation trends and concluded that SST trends have contributed to historical drying in East Africa.

Here, we leverage the eight CMIP model large ensembles to evaluate whether SST and SLP trend patterns related to regional precipitation trends (1979-2014) are similar to those shown in Section 3b. For each model ensemble member, we calculate the linear trend in SLP and SST at each gridpoint and the linear trend in precipitation in each region of interest (Table 2). We then separately regress the gridded SST and SLP trends against the regionally-averaged precipitation trend across ensemble members. Here we employ a two-tailed local t-test to test for significant correlations across each ensemble, and stipple SST at each gridpoint (and blacken SLP contours) where 5 or more models agree on statistically significant regression coefficients. The results are shown in Fig. 5 and are scaled by -1 to reflect SST trends that are correlated with drying in the boxed region. We note that applying the Wilks (2016) false discovery rate correction here would substantially reduce the statistical significance of our results; however, the small ensemble sizes for some models mean that genuinely robust signals may fail to reach significance using this statistical test framework. We performed a similar analysis and statistical significance testing on data from the longer pre-industrial simulations of the same CMIP models (not shown) and found the same patterns of SST and SLP with similar stippling for all of the regions shown in Fig. 5. This provides further evidence and confidence that multidecadal trend relationships between SST, SLP, and regional precipitation trends in Fig. 5 are robust.

In the southwestern and southeastern US there is a significant relationship between tropical Pacific SST trends and drying trends (Figs. 5a,b); together with the SLP trend contours, these patterns are reminiscent of the modeled ENSO-like teleconnections shown in Fig. 4, rows A and B for both regions. The negative precipitation trend in the southwestern US is also associated with a statistically significant positive SST trend in the central north Pacific (we elaborate on this result in further detail in the conclusion). Our analysis of the multidecadal variability in the pre-industrial control simulations from the same set of CMIP models (not shown) illustrates similar teleconnection patterns with similar model agreement, signifying that there exists robust patterns of SST trends in the tropical Pacific correlated to precipitation trends across both regions in forced and unforced simulations.

Near the Maritime Continent, local cooling SST trends and eastern Pacific warming trends are weakly related to the drying trend in the region, supported by a positive local SLP trend (Fig. 5d). The Amazon precipitation trends in FMAM and ASON also both show relationships to SST trends (Figs. 5f,g) that are unlike those seen on interannual timescales (Figs. 4F3,G3): in FMAM, drying trends are associated with a weak warming trend in the Pacific, while in ASON drying trends are associated with a noticeable inter-hemispheric SST gradient in the tropical Atlantic.

The other three regions (East Africa, subtropical South America, and the Sahel; Fig. 5c,e,j) also each show little to no statistically significant connection between tropical Pacific SST, SLP, and precipitation trends for their corresponding seasons. Note that our statistical constraint for

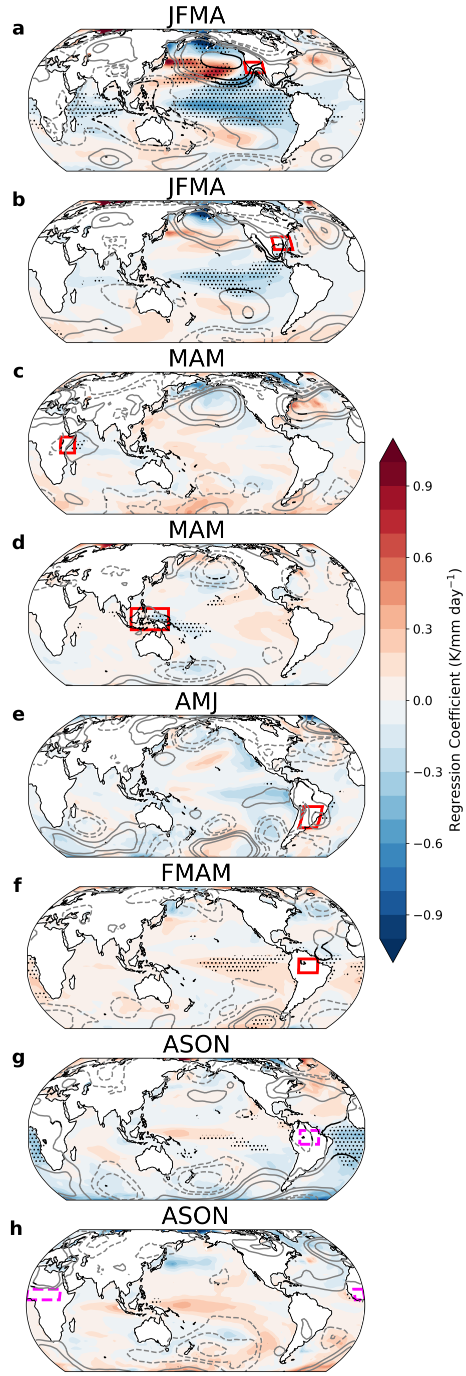

452 FIG. 5. Multidecadal trends in seasonal SST and SLP regressed against multidecadal trends in seasonal regional precipitation from each CMIP large ensemble. Trends in regional precipitation are calculated from the average over the red box in each plot. Significant relationships between SST trends and regional precipitation trends are stippled. Significant relationships between SLP trends and regional precipitation trends are contoured in black (otherwise grey). SLP contours correspond to (0.25, 0.5, 1, 3, and 5) hPa/mm/day (dashed contours are negative, zero contour is omitted). Regression values are scaled by -1 to facilitate comparison with the La-Niña-like SST pattern from Figure 2.

significant relationships between SST, SLP and regional precipitation trends is high; relaxing this constraint from 5 or more models with regression coefficients of $p<0.1$ to 5 or more models agreeing on the *sign* regression coefficient increases the geographical area of significant SST and SLP trends that are associated with these regions' precipitation trends. However, the associated multi-model mean relationships between SST, SLP, and regional precipitation trends to these areas are still weak.

In East Africa, the multidecadal drying trend in MAM is correlated with local cooling in the western Indian Ocean (Fig. 5c), a relationship that is also seen on interannual timescales in observations, and in the CMIP and AMIP models (Fig. 4 row C).

That CMIP models do not show a strong link between multidecadal SST trends and precipitation trends over the Maritime Continent and subtropical South America (Fig. 5e) is surprising, given that the ensemble-averaged precipitation trends for this regions in AMIP simulations (Fig. 3) more closely resembles observations those from CMIP simulations. Panels D3 and E3 in Fig. 4 demonstrate that CMIP models do simulate the observed interannual SST–precipitation teleconnections for the Maritime Continent and subtropical South America associated with ENSO. However, these interannual teleconnections are weaker in the CMIP and AMIP models than in observations, which likely contributes to a too-weak relationship between SSTs and precipitation on multidecadal timescales. It is also possible that the CMIP models' multidecadal SST variability never accesses the pattern of SST trends seen in observations (Wills et al. 2022), compromising the atmospheric response to these SST trends responsible for the multidecadal teleconnections to precipitation over the Maritime Continent and subtropical South America (see also Jacobson and Seager 2025). Indeed, results presented in the next section show that the observed trends in the Maritime Continent and subtropical South America are consistent with a scaled-up relationship between multidecadal ENSO-like SST anomalies and precipitation in these two regions. Other work has shown that the tropical Atlantic is responsible for multidecadal precipitation variability in subtropical South America (Seager et al. 2010a), but our results do not indicate a robust connection.

d. SST influence on regional precipitation trends

We have found that tropical Pacific SST trends are linked to precipitation trends in the southwestern and southeastern US on multidecadal timescales via ENSO-like teleconnections (Figs. 5A,B).

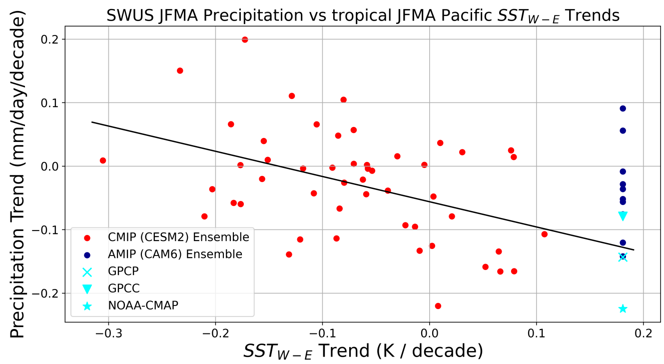

FIG. 6. Example of regressing precipitation trends against SST-gradient trends for the CESM2 Large Ensemble for the period 1979-2014. Red points indicate trends from each individual ensemble member, blue points indicate trends from the corresponding AMIP model (CAM6-GOGA simulation), and the green line is the regression fit to the large ensemble, extrapolated to the observed zonal SST gradient trend. The observed precipitation trends calculated from three precipitation products are shown in light blue, plotted at the value of the observed zonal SST gradient trend calculated from NOAAERSSTv5 data.

In this section, we regress simulated precipitation trends against simulated trends in the equatorial Pacific SST-gradient (SST_{W-E}, see Section 2c.4) to determine to what extent the CMIP models would represent the observed regional precipitation trends if they had simulated the observed amplitude of the SST trend pattern in the equatorial Pacific. Figure 6 shows an example of this regression for area-averaged precipitation trends in the southwestern US (JFMA) in the CESM2 Large Ensemble along with precipitation trends from its corresponding AMIP ensemble. Note that the regression line fit to the CESM2 data falls within the spread of the AMIP model's simulated precipitation trends and close to the observed precipitation trend when evaluated using the observed trend value of SST_{W-E}. Given that the AMIP model ensemble corresponding to CESM2 is driven by the observed zonal SST gradient trend, our regression result indicates that the equatorial Pacific zonal SST gradient trend is directly related to the precipitation trend in the southwestern US in this model.

For each region, we plot the area-averaged precipitation trend estimate for each CMIP model (labeled SST-Grad Regression) using our regression along with the simulated CMIP and AMIP model ensemble average trends in Fig. 7. The observed regional precipitation trends from the GPCP, GPCC, and NOAA CMAP products are plotted as dashed horizontal lines for comparison.

Comparing the SST-Grad Regression box to the CMIP box for each region shows whether or not the CMIP models would be able to simulate the observed precipitation trends if they had simulated the observed zonal SST gradient in the equatorial Pacific. The AMIP box represents the spread in precipitation trends models simulate given the observed evolution of global SSTs.

Taking into account the zonal SST-gradient trend helps reconcile the differences in simulated precipitation trends simulated by CMIP and AMIP models over the southwestern US and subtropical South America (Figs. 7a,e). In the southwestern US, strong relationships between equatorial Pacific SST and precipitation were identified on interannual and multidecadal timescales, and the results in Fig. 7a suggest equatorial Pacific SST trends are responsible for a majority of the observed drying in JFMA in this region. In subtropical South America, the SST gradient scaled precipitation trends help models capture the observed precipitation trends from GPCC and GPCP. The fact that AMIP models do not wholly simulate the observed precipitation trends, despite the influence of the observed SST pattern in this region, suggests that there are other influences on precipitation trends in this region across models.

Over the southeastern US and Maritime Continent (Fig. 7b,d), the SST-gradient scaled precipitation trends reconcile some of the difference between the CMIP and AMIP model precipitation trends. This result suggests that another process, unconnected to the atmosphere's response to the equatorial Pacific SST gradient, could be contributing to the observed precipitation trend in these two regions. For the Maritime Continent, this is surprising: Ghosh and Shepherd (2023) attribute long-term wetting trends in this region (although for a different season) to a strengthening equatorial Pacific SST gradient, although they acknowledge that changes in Indian Ocean SST could also affect the trends in precipitation. For the southeastern US, the SST-gradient scaled precipitation trends are able to explain some of the GPCC trend, but the other two products (GPCP and NOAA CMAP) as well as all of the AMIP model simulated trends lay out of reach of our SST-gradient metric.

In East Africa and the Amazon in FMAM, the SST-gradient scaled precipitation does not reconcile the differences between CMIP and AMIP models' precipitation trends, nor does it explain the observed precipitation trends in these regions. For the Amazon in FMAM, this is surprising considering that the CMIP models simulate a statistically significant relationship between tropical Pacific SST trends and preciptiation in this region. However, the AMIP models still simulate trends

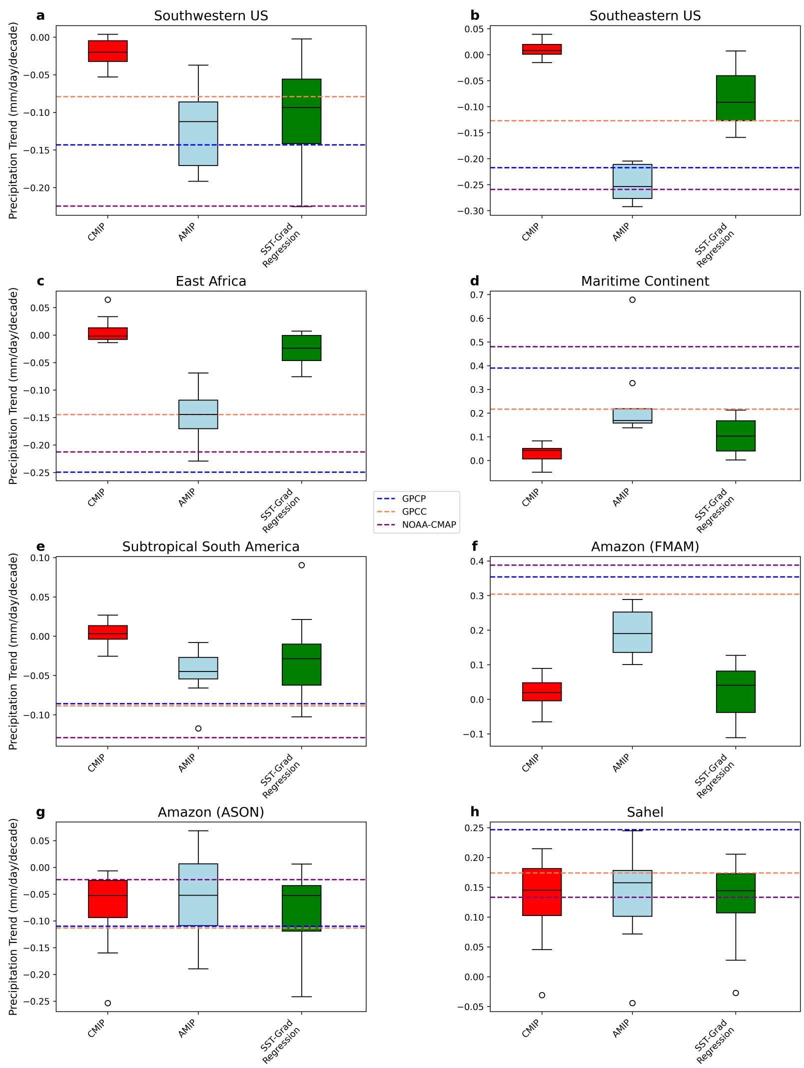

Fig. 7. Box and whisker plots illustrating the area-averaged trends for each region/season in Table 2 from CMIP (red) and AMIP (light blue) model ensemble averages, and the SST-gradient regression-estimated precipitation trend for each model(green). The horizontal dashed lines correspond to the observed precipitation trend from three different datasets, GPCP (blue), GPCC (coral) and NOAA CMAP (purple). The black line in each box represents the median. Circles represent flier points, which are data outside of the 1.5x inter-quartile range of the boxes. The box and whisker plots summarize results from 376 CMIP simulations, 44 AMIP simulations, and 8 CMIP-adjusted models.

closer to observations than the CMIP models (Fig. 3), which indicate that SST trends outside of the equatorial Pacific may be responsible for the observed precipitation trends in these regions.

e. Regions of agreement between AMIP and CMIP

Two regions of interest (the Sahel and the Amazon in ASON) show little difference between AMIP and CMIP simulated precipitation trends (boxed in dashed magenta in Fig. 3). Figures 7g-h show the inter-model spread in their precipitation trends simulated by CMIP and AMIP as well as the calculation from our SST gradient regression method; all three show agreement on the drying trend in the Amazon Rainforest and the wetting trend in the Sahel. The shared forced response in these two regions in both the CMIP and AMIP models, despite different SST trend patterns, suggests either that the precipitation trends in these two regions is due to local forcing (and entirely unrelated to SST trends), or that a common SST response to radiative forcing prescribed to both models is responsible for the precipitation trends.

Biasutti (2019) reviews the many hypotheses for the rebound in Sahel precipitation since the late 1970s, with the leading cause being the reduction of reflective aerosol emissions from European and North American factories. These emissions caused cooling over the North Atlantic, shifting the rain band over Western Africa southward (Folland et al. 1986; Giannini et al. 2003; Dong and Sutton 2015) away from the Sahel and led to a negative precipitation trend from 1950 to 1990. The identical aerosol emissions imposed on both CMIP and AMIP models could have led to this similar effect, as the reduction of emissions would lead to a large rebound in precipitation in the Sahel afterward as North Atlantic SSTs warm and the rain band shifts northward.

The Amazonian drying trend in ASON may also be related to SST trends. The common characteristic between AMIP and CMIP SST trends in the Atlantic is a meridional SST gradient (Figs. 2d,h) that indicates a northward ITCZ shift over the Atlantic, which would decrease convection and rainfall over the Amazon and subsequently promote drying in this region (Knight et al. 2008; Harris et al. 2008).

4. Conclusions and Implications

In this paper, we compared the precipitation responses of AMIP and CMIP model ensembles under historical forcing to observed precipitation trends around the world over 1979-2014. CMIP models fail to simulate the observed precipitation trends in most regions, while AMIP models generally produce more accurate trends. Comparing results from CMIP and AMIP models suggests that observed SST trends that are distinct from those found in the forced response of CMIP models have contributed to the observed precipitation trends in the southwestern US (JFMA, consistent with Lehner et al. 2018; Qiu et al. 2024; Kuo et al. 2025), the southeastern US (JFMA), the Maritime Continent (MAM), the Amazon (FMAM), East Africa (MAM), and subtropical South America (AMJ, consistent with Seager et al. 2010a) (see Table 2).

The multidecadal JFMA drying trends in the southwestern US and subtropical South America showed a strong relationship to the trend in the zonal SST gradient in the equatorial Pacific, likely via teleconnections similar to those observed in interannual La Niña events (see also Lehner et al. 2018; Seager et al. 2010b). Recent work (Klavans et al. 2025) has concluded that SST trends from the North Pacific have also contributed to historical drying in the southwestern US by statistically correcting CMIP models' forced climate variability, but further work may be needed to elucidate a physical mechanism to support their claim.

The observed trends in Maritime Continent and southeastern US precipitation also show a relationship to the trend in the zonal SST-gradient trend in the equatorial Pacific, although not as strongly as in the southwestern US and subtropical South America. We find that models simulate strong interannual teleconnections between equatorial Pacific SST and Maritime Continent precipitation, but significantly weaker teleconnections that shift west on multidecadal timescales. Models simulate interannual and multidecadal teleconnections from tropical Pacific SSTs to southeastern US precipitation, but observations disagree on a strong teleconnection from this region on interannual timescales, calling into question the significance of the multidecadal teleconnection we identified in Section 3c. While previous work has attributed Maritime Continent precipitation trends to tropical Pacific SST trends (Ghosh and Shepherd 2023), less has been done to connect the tropical Pacific to the southeastern US on decadal and longer timescales.

Although the observed multidecadal SST trends (not seen in the forced response from the CMIP models) contribute to the precipitation trends over East Africa (MAM) and the Amazon (FMAM), those precipitation trends cannot be totally attributed to differences in trends in the equatorial Pacific zonal SST gradient. This is surprising for the Amazon (FMAM), where positive precipitation anomalies are strongly linked to La Niña events on interannual timescales, which feature anomalies in the zonal SST gradient that are similar to the observed multidecadal trend in the Pacific.

CMIP and AMIP models simulated similar precipitation trends to the observed trends, in both the Sahel and Amazon in ASON. This finding suggests either that the long-term precipitation changes may scale more directly with forcing or global temperature in these two regions, in which case they may be less sensitive to how SST patterns may change in the future, or that CMIP and AMIP models share a sufficiently similar pattern of SST trend to observations. For the Amazon, there is a common SST trend pattern that features more warming in the northern subtropical Atlantic than in the southern subtropical Atlantic. It is possible that this pattern of warming is the result of long-term reduction of aerosol emissions from Europe and North America, leading to a meridional SST gradient (see Figure 2d,h) that shifted the ITCZ northward (Biasutti 2019), drying the Amazon and wetting the Sahel and over 1979-2014.

The sign of the trend in the equatorial Pacific zonal SST gradient could change in the future, eventually becoming more El-Niño-like with enhanced warming in the east Pacific (Rugenstein et al. 2020; Armour et al. 2024; Forster et al. 2021; Tierney et al. 2019). Our regressions of precipitation trends against the equatorial Pacific SST gradient in CMIP models (Section 3d) suggest that if this SST pattern change does occur, the southwestern US, the southeastern US, and subtropical South America could each become substantially wetter while the Maritime Continent could become drier. Only if the recent tropical Pacific SST trend pattern continues, as suggested in Jiang et al. (2024), would we expect future precipitation trends in these regions to be similar to those observed over recent decades. These results suggest that extrapolating observed precipitation trends using the assumption that they scale with global average temperature (e.g., Kravitz et al. 2017; Kravitz and Snyder 2023; Herger et al. 2015) could lead to substantial errors in regional precipitation projections.

Acknowledgments. J.R.P., K.C.A., and D.S.B were supported by National Science Foundation (NSF) Award AGS-2203543. J.R.P. and D.S.B. were supported by NSF award AGS-2128409 and the Tamaki Foundation. K.C.A. was supported by a Calvin Professorship in Oceanography. We thank Robert Jnglin Wills for insightful discussions of this work, and three anonymous reviewers for helpful comments regarding the manuscript.

Data availability statement. The model data used in the analysis can be found in the Earth System Grid Federation (https://esgf.github.io) or in the NCAR Climate Data Gateway (https://www.earthsystemgrid.org). Observational data (GPCP, GPCC, NOAA CMAP, and NOAAERSSTv5 datasets) were downloaded from NOAA's Physical Science Laboratory (https://psl.noaa.gov/).

References

Adam, J., A. Hamlet, and D. Lettenmaier, 2009: Implications of global climate change for snowmelt hydrology in the twenty-first century. *Hydrol. Process*, **23**, 962–972, https://doi.org/10.1002/hyp.7201.

Adler, R., and Coauthors, 2018: The Global Precipitation Climatology Project (GPCP) monthly analysis (new version 2.3) and a review of 2017 global precipitation. *Atmosphere*, **9**, 138, https://doi.org/10.3390/atmos9040138.

Almeida, C., J. Oliveira-Junior, R. Delgado, P. Cubo, and M. Ramos, 2016: Spatiotemporal rainfall and temperature trends throughout the Brazilian Legal Amazon, 1973-2013. *Int. J. Climatol.*, **37**, 2013–2026, https://doi.org/10.1002/joc.4831.

Armour, K., and Coauthors, 2024: Sea-surface temperature pattern effects have slowed global warming and biased warming-based constraints on climate sensitivity. *Proc. Natl. Acad. Sci. U.S.A.*, **121**, https://doi.org/10.1073/pnas.2312093121.

Benjamini, Y., and Y. Hochberg, 1995: Controlling the false discovery rate: a practical and powerful approach to multiple testing. *J. R. Stat. Soc., B: Stat. Methodol.*, **57**, 289–300, https://doi.org/10.1111/j.2517-6161.1995.tb02031.x.

Biasutti, M., 2019: Rainfall trends in the African Sahel: Characteristics, processes, and causes. *WIREs Clim Change*, https://doi.org/10.1002/wcc.591.

Blackport, R., and J. Fyfe, 2022: Climate models fail to capture strengthening wintertime North Atlantic jet and impacts on Europe. *Sci. Adv.*, **8**, https://doi.org/10.1126/sciadv.abn3112.

Bracegirdle, T. J., H. Lu, R. Eade, and T. Woollings, 2018: Do CMIP5 models reproduce observed low-frequency North Atlantic jet variability? *Geophys. Res. Lett.*, **45**, 7204–7212, https://doi.org/10.1029/2018GL078965.

Cayan, D., T. Das, D. Pierce, T. Barnett, M. Tyree, and A. Gershunov, 2010: Future dryness in the southwest US and the hydrology of the early 21st century drought. *Proc. Natl. Acad. Sci.*, **107**, 21 271–21 276, https://doi.org/10.1073/pnas.0912391107.

Chemke, R., Y. Ming, and J. Yuval, 2022: The intensification of winter mid-latitude storm tracks in the Southern Hemisphere. *Nat. Clim. Chang.*, **12**, 553–557, https://doi.org/10.1038/s41558-022-01368-8.

Chung, E.-S., A. Timmermann, B. Soden, K.-J. Ha, L. Shi, and V. John, 2019: Reconciling opposing Walker circulation trends in observations and model projections. *Nat. Clim. Chang.*, **9**, 405–412, https://doi.org/10.1038/s41558-019-0446-4.

Cinquini, L., and Coauthors, 2014: The Earth System Grid Federation: An open infrastructure for access to distributed geospatial data. *Future Generation Computer Systems*, **36**, 400–417, https://doi.org/10.1016/j.future.2013.07.002.

Davey, M., A. Brookshaw, and S. Ineson, 2014: The probability of the impact of ENSO on precipitation and near-surface temperature. *Clim. Risk. Manag.*, **1**, 5–24, https://doi.org/10.1016/j.crm.2013.12.002.

Delworth, T. L., F. Zeng, A. Rosati, G. Vecchi, and A. Wittenberg, 2015: A link between the hiatus in global warming and North American drought. *J. Climate*, **28**, 3834–3845, https://doi.org/10.1175/JCLI-D-14-00616.1.

Donat, M. G., C. Delgado-Torres, P. De Luca, R. Mahmood, P. Ortega, and F. J. Doblas-Reyes, 2023: How credibly do CMIP6 simulations capture historical mean and extreme precipitation changes? *Geophys. Res. Lett.*, **50**, https://doi.org/10.1029/2022GL102466.

Doney, S., and Coauthors, 2012: Climate change impacts on marine ecosystems. *Annu. Rev. Mar. Sci.*, **4**, 11–37, https://doi.org/10.1146/annurev-marine-041911-111611.

Dong, B., and R. Sutton, 2015: Dominant role of greenhouse-gas forcing in the recovery of Sahel rainfall. *Nature Clim Change*, **5**, 757–760, https://doi.org/10.1038/nclimate2664.

Douville, H., and Coauthors, 2021: Water cycle changes. *Climate Change 2021: The Physical Science Basis. Contribution of Working Group I to the Sixth Assessment Report of the Intergovernmental Panel on Climate Change*, V. Masson-Delmotte, P. Zhai, A. Pirani, S. Connors, C. Péan, S. Berger, N. Caud, Y. Chen, L. Goldfarb, M. Gomis, M. Huang, K. Leitzell, E. Lonnoy, J. Matthews, T. Maycock, T. Waterfield, O. Yelekçi, R. Yu, and B. Z. (eds.), Eds., Cambridge University Press, 1055–1210, https://doi.org/10.1017/9781009157896.010.

Easterling, D., and Coauthors, 2017: Precipitation change in the United States. *Fourth National Climate Assessment*, https://doi.org/10.7930/J0H993CC.

Eyring, V., S. Bony, G. Meehl, C. Senior, B. Stevens, R. J. Stouffer, and K. Taylor, 2016: Overview of the Coupled Model Intercomparison Project Phase 6 (CMIP6) experimental design and organization. *GeoSci. Model Dev.*, **9**, 1937–1958, https://doi.org/https://doi.org/10.5194/gmd-9-1937-2016.

Fan, T., C. Deser, and D. Schneider, 2014: Recent Antarctic sea ice trends in the context of Southern Ocean surface climate variations since 1950. *Geophys. Res. Lett.*, **41**, 2419–2426, https://doi.org/10.1002/2014GL059239.

Folland, C., J. Owen, M. Ward, and A. Colman, 1991: Prediction of seasonal rainfall in the Sahel region using empirical and dynamical methods. *J. Forecast*, **10**, 21–56, https://doi.org/10.1002/for.3980100104.

Folland, C., T. Palmer, and D. Parker, 1986: Sahel rainfall and worldwide sea temperatures, 1901–85. *Nature*, **320**, 602–607, https://doi.org/10.1038/320602a0.

Forster, P., and Coauthors, 2021: The Earth's energy budget, climate feedbacks, and climate sensitivity. *Climate Change 2021: The Physical Science Basis. Contribution of Working Group I to the Sixth Assessment Report of the Intergovernmental Panel on Climate Change*, V. Masson-Delmotte, P. Zhai, A. Pirani, S. Connors, C. Péan, S. Berger, N. Caud, Y. Chen, L. Goldfarb, M. Gomis, M. Huang, K. Leitzell, E. Lonnoy, J. Matthews, T. Maycock, T. Waterfield, O. Yelekçi, R. Yu, and B. Z. (eds.), Eds., Cambridge University Press, 923–1054, https://doi.org/10.1017/9781009157896.009.

Garreaud, R., and D. Battisti, 1999: Interannual (ENSO) and interdecadal (ENSO-like) variability in the Southern Hemisphere tropospheric circulation. *J. Climate*, **12**, 2113–2123, https://doi.org/10.1175/1520-0442(1999)012⟨2113:IEAIEL⟩2.0.CO;2.

Gebrechorkos, S., S. Hülsmann, and C. Bernhofer, 2019: Long-term trends in rainfall and temperature using high-resolution climate datasets in East Africa. *Sci Rep*, **9 (11376)**, https://doi.org/10.1038/s41598-019-47933-8.

Ghosh, R., and T. Shepherd, 2023: Storylines of Maritime Continent dry period precipitation changes under global warming. *Environ. Res. Lett.*, **18 (3)**, 034 017, https://doi.org/10.1088/1748-9326/acb788.

Giannini, A., R. Saravanan, and P. Chang, 2003: Oceanic forcing of Sahel rainfall on interannual to interdecadal time scales. *Science*, **302**, 1027–1030, https://doi.org/10.1126/science.1089357.

Gloor, M., and Coauthors, 2015: Recent Amazon climate as background for possible ongoing and future changes of Amazon humid forests. *Global Biogeochem. Cycles*, **29**, 1384–1399, https://doi.org/10.1002/2014GB005080.

Gu, G., and R. Adler, 2023: Observed variability and trends in global precipitation during 1979–2020. *Clim. Dyn.*, **61**, 131–150, https://doi.org/10.1007/s00382-022-06567-9.

Harris, P., C. Huntingford, and P. Cox, 2008: Amazon Basin climate under global warming: the role of the sea surface temperature. *Phil. Trans. R. Soc. B*, **363**, 1753–1759, https://doi.org/10.1098/rstb.2007.0037.

Hazeleger, W., and Coauthors, 2010: EC-Earth: a seamless earth-system prediction approach in action. *Bull. Amer. Meteor. Soc.*, **91**, 1357–1364, https://doi.org/10.1175/2010BAMS2877.1.

Herger, N., B. M. Sanderson, and R. Knutti, 2015: Improved pattern scaling approaches for the use in climate impact studies. *Geophysical Research Letters*, **42 (9)**, 3486–3494, https://doi.org/https://doi.org/10.1002/2015GL063569.

Hersbach, H., and Coauthors, 2020: The ERA5 global reanalysis. *Q J R Meterol Soc*, **146**, 1999–2049, https://doi.org/10.1002/qj.3803.

Hoerling, M., J. Eischeid, and J. Perlwitz, 2010: Regional precipitation trends: Distinguishing natural variability from anthropogenic forcing. *J. Climate*, **23**, 2131–2145, https://doi.org/10.1175/2009JCLI3420.1.

Huang, B., and Coauthors, 2017: Extended Reconstructed Sea Surface Temperature, version 5 (ERSSTv5): Upgrades, validations, and intercomparisons. *J. Climate*, **30**, 8179–8205, https://doi.org/10.1175/JCLI-D-16-0836.1.

Jacobson, T., and R. Seager, 2025: Pacific decadal variability and its hydroclimate teleconnections in CMIP6 models. *J. Climate*, **38**, 5103–5127, https://doi.org/10.1175/JCLI-D-24-0616.1.

Jiang, F., R. Seager, and M. Cane, 2024: A climate change signal in the tropical Pacific emerges from decadal variability. *Nat. Commun.*, **15**, 8291, https://doi.org/10.1038/s41467-024-52731-6.

Kang, J., T. Shaw, S. Kang, I. Simpson, and Y. Yu, 2024: Revisiting the reanalysis-model discrepancy in Southern Hemisphere winter storm track trends. *npj Clim. Atmos. Sci.*, **7**, 252, https://doi.org/10.1038/s41612-024-00801-3.

Kang, J., R. Thomas, N. Dunstone, T. Shaw, and T. Woolings, 2025: Robust impact of tropical Pacific SST trends on global and regional circulation in boreal winter. *npj Clim Atmos Sci*, **8**, 315, https://doi.org/10.1038/s41612-025-01192-9.

Kay, J., and Coauthors, 2015: The Community Earth System Model (CESM) Large Ensemble Project: A community resource for studying climate change in the presence of internal climate variability. *Bull. Amer. Meteor. Soc.*, **96**, 1333–1349, https://doi.org/10.1175/BAMS-D-13-00255.1.

Kirchmeier-Young, M., F. Zwiers, and N. Gillett, 2017: Attribution of extreme events in Arctic sea ice extent. *J. Climate*, **30**, 553–571, https://doi.org/10.1175/JCLI-D-16-0412.1.

Klavans, J., P. DiNezio, A. Clement, C. Deser, T. Shanahan, and M. Cane, 2025: Human emissions drive recent trends in north Pacific climate variations. *Nature*, **644**, 684–692, https://doi.org/10.1038/s41586-025-09368-2.

Knight, J. R., C. Folland, and A. Scaife, 2008: Climate impacts of the Atlantic Multidecadal Oscillation. *Geophys. Res. Lett.*, **33**, https://doi.org/10.1029/2006GL026242.

Knutson, T., and F. Zeng, 2018: Model assessment of observed precipitation trends over land regions: Detectable human influences and possible low bias in model trends. *J. Climate*, **31**, 4617–4637, https://doi.org/10.1175/JCLI-D-17-0672.1.

Kociuba, G., , and S. B. Power, 2015: Inability of CMIP5 models to simulate recent strengthening of the Walker circulation: Implications for projections. *J. Climate*, **28**, 20–35, https://doi.org/10.1175/JCLI-D-13-00752.1.

Konapala, G., A. Mishra, Y. Wada, and M. Mann, 2020: Climate change will affect global water availability through compounding changes in seasonal precipitation and evaporation. *Nat Commun*, **11**, 3044, https://doi.org/10.1038/s41467-020-16757-w.

Kravitz, B., C. Lynch, C. Hartin, and B. Bond-Lamberty, 2017: Exploring precipitation pattern scaling methodologies and robustness among CMIP5 models. *Geosci. Model Dev.*, **10**, 1889–1902, https://doi.org/10.5194/gmd-10-1889-2017.

Kravitz, B., and A. Snyder, 2023: Pangeo-enabled ESM pattern scaling (PEEPS): A customizable dataset of emulated Earth System Model output. *PLOS Climate*, **12**, https://doi.org/10.1371/journal.pclm.0000159.

Kuo, Y., H. Kim, and F. Lehner, 2023: Anthropogenic aerosols contribute to the recent decline in precipitation over the U.S. southwest. *Geophysical Research Letters*, **50 (23)**, e2023GL105 389, https://doi.org/https://doi.org/10.1029/2023GL105389.

Kuo, Y., and Coauthors, 2025: Recent southwestern U.S. drought exacerbated by anthropogenic aerosols and tropical ocean warming. *Nat. Geosci.*, **18**, 578–585, https://doi.org/10.1038/s41561-025-01728-x.

Lehner, F., C. Deser, I. Simpson, and L. Terray, 2018: Attributing the U.S. Southwest's recent shift into drier conditions. *Geophys. Res. Lett.*, **45**, 6251–6261, https://doi.org/10.1029/2018GL078312.

Maher, N., and Coauthors, 2019: The Max Planck Institute Grand Ensemble: Enabling the exploration of climate system variability. *JAMES*, **11**, 2050–2069, https://doi.org/10.1029/2019MS001639.

Moreira, R., B. dos Santos, T. Biggs, F. de Sales, and S. Sieber, 2024: Identifying clusters of precipitation for the Brazilian Legal Amazon based on magnitude of trends and its correlation with sea surface temperature. *Sci Rep*, **14**, https://doi.org/10.1038/s41598-024-63583-x.

Olonscheck, D., and Coauthors, 2023: The new Max Planck Institute Grand Ensemble with CMIP6 forcing and high-frequency model output. *JAMES*, **15**, https://doi.org/10.1029/2023MS003790.

Qian, J., B. Viner, S. Noble, D. Werth, J. Wermter, S. Chiswell, and C. Li, 2024: Understanding observed precipitation change and the new climate normal from the perspective of daily weather types in the Southeast United States. *J. Climate*, https://doi.org/10.1175/JCLI-D-23-0367.1.

Qiu, W., M. Collins, A. A. Scaife, and A. Santoso, 2024: Tropical Pacific trends explain the discrepancy between observed and modelled rainfall change over the Americas. *npj Clim. Atmos. Sci.*, **7**, 201, https://doi.org/10.1038/s41612-024-00750-x.

Rodgers, K., and Coauthors, 2021: Ubiquity of human-induced changes in climate variability. *Earth Syst. Dynam.*, **12**, 1393–1411, https://doi.org/10.5194/esd-12-1393-2021.

Ropelewski, C., and M. Halpert, 1987: Global and regional scale precipitation patterns associated with the El Niño/Southern Oscillation. *Mon. Wea. Rev.*, **115**, 1606–1626, https://doi.org/10.1175/1520-0493(1987)115⟨1606:GARSPP⟩2.0.CO;2.

Rowell, D. P., B. B. B. Booth, S. E. Nicholson, and P. Good, 2015: Reconciling past and future rainfall trends over East Africa. *J. Climate*, **28**, 9768–9788, https://doi.org/10.1175/JCLI-D-15-0140.1.

Rugenstein, M., J. Bloch-Johnson, J. Gregory, T. Andrews, T. Mauritsen, C. Li, and et al., 2020: Equilibrium climate sensitivity estimated by equilibrating climate models. *Geophys. Res. Lett.*, **47**, https://doi.org/10.1029/2019GL083898.

Schneider, U., S. Hänsel, P. Finger, E. Rustemeier, and M. Ziese, 2022: GPCC full data monthly product version 2022 at 2.5°: Monthly land-surface precipitation from rain-gauges built on GTS-based and historical data. https://doi.org/10.5676/DWD_GPCC/FD_M_V2022_250.

Schwalm, C., S. Glendon, and P. Duffy, 2020: RCP8.5 tracks cumulative CO_2 emissions. *Proc. Natl. Acad. Sci. U.S.A.*, **117 (33)**, 19 656–19 657, https://doi.org/10.1073/pnas.2007117117.

Schwarzwald, K., and R. Seager, 2024: Revisiting the ”East African Paradox”: CMIP6 models also struggle to reproduce strong observed long rain drying trends. *J. Climate*, **37**, 6641–6658, https://doi.org/10.1175/JCLI-D-24-0225.1.

Seager, R., and M. Hoerling, 2014: Atmosphere and ocean origins of North American droughts. *J. Climate*, **27**, 4581–4606, https://doi.org/10.1175/JCLI-D-13-00329.1.

Seager, R., N. Naik, W. Baethgen, A. Robertson, Y. Kushnir, J. Nakamura, and S. Jurburg, 2010a: Tropical oceanic causes of interannual to multidecadal precipitation variability in Southeast South America over the past century. *J. Climate*, **23**, 5517–5539, https://doi.org//10.1175/2010JCLI3578.1.

Seager, R., N. Naik, M. Ting, M. Cane, N. Harnik, and Y. Kushnir, 2010b: Adjustment of the atmospheric circulation to tropical Pacific sst anomalies: Variability of transient eddy propagation in the Pacific–North America sector. *Q.J.R. Meteorol. Soc.*, **136**, 277–296, https://doi.org/10.1002/qj.588.

Seager, R., M. Ting, P. Alexander, H. Liu, J. Nakamura, C. Li, and M. Newman, 2023: Ocean-forcing of cool season precipitation drives ongoing and future decadal drought in southwestern North America. *npj Clim Atmos Sci*, **6**, 141, https://doi.org/10.1038/s41612-023-00461-9.

Seager, R., and G. Vecchi, 2010: Greenhouse warming and the 21st century hydroclimate of southwestern North America. *Proc. Natl. Acad. Sci. U.S.A.*, **107 (50)**, 21 277–21 282, https://doi.org/10.1073/pnas.0910856107.

Seneviratne, S., T. Corti, E. Davin, M. Hirschi, E. Jaeger, I. Lehner, B. Orlowsky, and A. Teuling, 2010: Investigating soil moisture–climate interactions in a changing climate: A review. *Earth-Sci. Rev.*, **99**, 125–161, https://doi.org/10.1016/j.earscirev.2010.02.004.

Shaw, T., O. Miyawaki, and A. Donohoe, 2022: Stormier Southern Hemisphere induced by topography and ocean circulation. *Proc. Natl. Acad. Sci. U.S.A.*, **119 (50)**, https://doi.org/10.1073/pnas.2123512119.

Shin, S.-I., and P. Sardeshmukh, 2011: Critical influence of the pattern of tropical ocean warming on remote climate trends. *Clim Dyn*, **36**, 1577–1591, https://doi.org/10.1007/s00382-009-0732-3.

Siler, N., C. Proistosescu, and S. Po-Chedley, 2019: Natural variability has slowed the decline in western U.S. snowpack since the 1980s. *Geophys. Res. Lett.*, **46**, 346–355, https://doi.org/10.1029/2018GL081080.

Simpson, I., and Coauthors, 2025: Confronting Earth system model trends with observations. *Sci. Adv.*, **11 (11)**, eadt8035, https://doi.org/10.1126/sciadv.adt8035.

Sun, L., M. Alexander, and C. Deser, 2018: Evolution of the global coupled climate response to Arctic sea ice loss during 1990–2090 and its contribution to climate change. *J. Climate*, **31**, 7823–7843, https://doi.org/10.1175/JCLI-D-18-0134.1.

Tatebe, H., and Coauthors, 2019: Description and basic evaluation of simulated mean state, internal variability, and climate sensitivity in MIROC6. *Geosci. Model Dev.*, **12**, 2727–2765, https://doi.org/10.5194/gmd-12-2727-2019.

Taylor, K. E., R. J. Stouffer, and G. A. Meehl, 2012: An overview of CMIP5 and the experiment design. *Bull. Amer. Metero. Soc.*, **93**, 485–498, https://doi.org/https://doi.org/10.1175/BAMS-D-11-00094.1.

Tierney, J. E., A. M. Haywood, R. Feng, T. Bhattacharya, and B. L. Otto-Bliesner, 2019: Pliocene warmth consistent with greenhouse gas forcing. *Geophys. Res. Lett.*, **46**, 9136–9144, https://doi.org/10.1029/2019GL083802.

Trenberth, K., G. Branstator, D. Karoly, A. Kumar, N. Lau, and C. Ropolewski, 1998: Progress during TOGA in understanding and modeling global teleconnections associated with tropical sea surface temperatures. *J. Geophys. Res.*, **103**, 14,291–14,324, https://doi.org/10.1029/97JC01444.

Vicente-Serrano, S. M., and Coauthors, 2022: Do CMIP models capture long-term observed annual precipitation trends? *Clim. Dyn.*, **58 (9)**, 2825–2842, https://doi.org/10.1007/s00382-021-06034-x.

von Salzen, K., and Coauthors, 2013: The Canadian Fourth Generation Atmospheric Global Climate Model (CanAM4). Part I: Representation of Physical Processes. *Atmosphere Ocean*, **51 (1)**, 104–125, https://doi.org/10.1080/07055900.2012.755610.

Weltzin, J., and Coauthors, 2003: Assessing the response of terrestrial ecosystems to potential changes in precipitation. *BioScience*, **53**, 941–952, https://doi.org/10.1641/0006-3568(2003)053[0941:ATROTE]2.0.CO;2.

Wilks, D. S., 2016: ”the stippling shows statistically significant grid points”: How research results are routinely overstated and overinterpreted, and what to do about it. *Bull. Amer. Meteor. Soc.*, **97**, 2263–2273, https://doi.org/10.1175/BAMS-D-15-00267.1.

Williams, A., B. Cook, and J. Smerdon, 2022: Rapid intensification of the emerging southwestern North American megadrought in 2020–2021. *Nat. Clim. Chang.*, **12**, 232–234, https://doi.org/https://doi.org/10.1038/s41558-022-01290-z.

Wills, R., Y. Dong, C. Proistosescu, K. Armour, and D. Battisti, 2022: Systematic climate model biases in the large-scale patterns of recent sea-surface temperature and sea-level pressure change. *Geophys. Res. Lett.*, **49**, https://doi.org/10.1029/2022GL100011.

Xie, P., and P. Arkin, 1997: Global precipitation: A 17-year monthly analysis based on gauge observations, satellite estimates, and numerical model outputs. *Bull. Amer. Metero. Soc.*, **78**, 2539–2558, https://doi.org/10.1175/1520-0477(1997)078⟨2539:GPAYMA⟩2.0.CO;2.

Yeager, S. G., and Coauthors, 2023: Reduced Southern Ocean warming enhances global skill and signal-to-noise in an eddy-resolving decadal prediction system. *npj Clim. Atmos. Sci.*, **6**, 107, https://doi.org/10.1038/s41612-023-00434-y.

Zhao, M., and T. Knutson, 2024: Crucial role of sea surface temperature warming patterns in near-term high-impact weather and climate projection. *npj Clim. Atmos. Sci.*, **7 (130)**, https://doi.org/10.1038/s41612-024-00681-7.